Benchmarking of Constant Power Generation Strategies for Single-Phase Grid-Connected Photovoltaic Systems

Ariya Sangwongwanich, *Student Member, IEEE*, Yongheng Yang, *Member, IEEE*, Frede Blaabjerg, *Fellow, IEEE*, and Huai Wang, *Senior Member, IEEE*

***Abstract*—With a still increase of grid-connected photovoltaic (PV) systems, challenges have been imposed on the grid due to the continuous injection of a large amount of fluctuating PV power, like overloading the grid infrastructure (e.g., transformers) during peak power production periods. Hence, advanced active power control methods are required. As a cost-effective solution to avoid overloading, a constant power generation (CPG) control scheme by limiting the feed-in power has been introduced into the currently active grid regulations. In order to achieve a CPG operation, this paper presents three CPG strategies based on a power control method (P-CPG), a current limit method (I-CPG), and the perturb and observe algorithm (P&O-CPG). However, the operational mode changes (e.g., from the maximum power point tracking to a CPG operation) will affect the entire system performance. Thus, a benchmarking of the presented CPG strategies is also conducted on a 3-kW single-phase grid-connected PV system. Comparisons reveal that either the P-CPG or I-CPG strategies can achieve fast dynamics and satisfactory steady-state performance. In contrast, the P&O-CPG algorithm is the most suitable solution in terms of high robustness, but it presents poor dynamic performance.**

***Index Terms*—Active power control, constant power control, maximum power point tracking (MPPT), photovoltaic (PV) systems, power converters.**

I. Introduction

PHOTOVOLTAIC (PV) systems have a high growth rate during the last several years and will play an even more significant role in the future mixed power grid [1]–[3]. A majority of PV systems are connected to the distribution grid (i.e., mainly single-phase systems) [2], where a maximum power point tracking (MPPT) is currently mandatory in most of the active grid codes, and also to ensure the maximum energy yield from the solar power [4]. At a high penetration level of PV systems in the near future, the grid may face a challenge of overloading during peak power generation periods through a day if the power capacity of the grid remains the same [5]–[7]. For instance, it was reported by BBC that parts of the Northern Ireland's grid were overloaded by the increased number of grid-connected PV systems in a sunny and clear day with strong solar irradiance [8]. In order to enable more PV installations and address such issues, the control algorithms have to be feasible to flexibly regulate the active power generated by PV systems [4], [9]–[12]. For instance, limiting the feed-in power of PV systems to a certain level has been found as an effective approach to overcome overloading [10], and thus, it is currently required in Germany through the grid codes [13], where it is stated that newly installed PV systems with a rated power below 30 kWp have to be able to limit its maximum feed-in power (i.e., 70% of the rated power) unless it can be remotely controlled. In fact, this active power control strategy corresponds to an absolute power constraint defined in the Danish grid code [14], and it is also referred to as a constant power generation (CPG) control in the prior-art work [15].

Actually, there are several methods to limit the feed-in power of the PV system in order to achieve a constant power production (e.g., integrating energy storage systems, installing dump load) [16]. However, the most intuitive and cost-effective way to achieve the CPG control is through the modification of the MPPT algorithm at the PV inverter level (also called power curtailment) and will be considered in this paper [17]. In this approach, the PV system continues operating in the MPPT mode with injection of the maximum power as long as the available PV power P_{MPPT} is below the set point P_{limit}. However, when the available power reaches the level of P_{limit}, the PV system will inject a constant active power, i.e., $P_{\text{pv}} = P_{\text{limit}}$. The operational principle of the CPG scheme can be illustrated in Fig. 1 and summarized as

$$P_{\text{pv}} = \begin{cases} P_{\text{MPPT}}, & \text{when} \quad P_{\text{MPPT}} \leq P_{\text{limit}} \\ P_{\text{limit}}, & \text{when} \quad P_{\text{MPPT}} > P_{\text{limit}} \end{cases} \tag{1}$$

where P_{pv} is the PV output power, P_{MPPT} is the maximum available power (according to the MPPT operation), and P_{limit}

Manuscript received April 15, 2016; revised June 29, 2016; accepted September 28, 2016. Date of publication August 16, 2017; date of current version January 18, 2018. Paper 2016-SECSC-0338.R1, presented at the 2016 IEEE Applied Power Electronics Specialists Conference, Long Beach, CA, USA, Mar. 20–24, and approved for publication in the IEEE TRANSACTIONS ON INDUSTRY APPLICATIONS by the Sustainable Energy Conversion Systems Committee of the IEEE Industry Applications Society. This work was supported in part by the European Commission within the European Unions Seventh Frame-work Program (FP7/2007-2013) through the SOLAR-ERA.NET Transnational Project (PV2.3-PV2GRID), by Energinet.dk (ForskEL, Denmark) under Project 2015-1-12359, and in part by the Research Promotion Foundation (Cyprus) under Project KOINA/SOLAR-ERA.NET/0114/02. *(Corresponding author: Yongheng Yang.)*

The authors are with the Department of Energy Technology, Aalborg University, Aalborg DK-9220, Denmark (e-mail: ars@et.aau.dk; yoy@et.aau.dk; fbl@et.aau.dk; hwa@et.aau.dk).

Color versions of one or more of the figures in this paper are available online at http://ieeexplore.ieee.org.

Digital Object Identifier 10.1109/TIA.2017.2740380

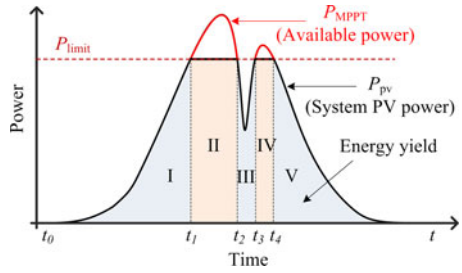

Fig. 1. CPG concept for PV systems. MPPT mode during I, III, V. CPG mode during II, IV [15].

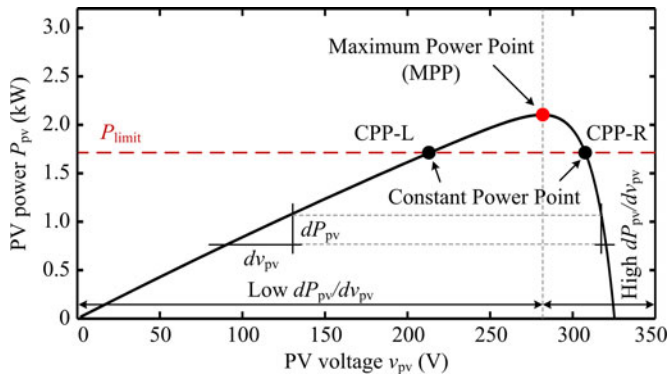

Fig. 2. Possible operating points of the PV system in the power–voltage curve of the PV arrays during the CPG operation (i.e., CPP) at a certain level of power limit P_{limit} and irradiance.

is the power limit, which is the set point. The constant power production can be achieved by regulating the PV output power at the operating point below the maximum power point (MPP), as it is shown in Fig. 2, and this operating point is called the constant power point (CPP) in this paper [18].

In the prior-art work, several CPG strategies for PV systems have been introduced. In fact, more methods have also been proposed for other applications (e.g., frequency regulation and low-voltage ride through), but they can also be applied to achieve the CPG control as well. Accordingly, the CPG strategies presented in the literature can be generally classified into three different approaches. In [15] and [19]–[22], the CPG control is realized by directly regulating the PV power to be constant through the closed-loop power control. This can be implemented either at the dc–dc stage [15], [19], [22], where the boost converter is controlled directly, or at the dc–ac stage [20], [21], where a constant power reference P_{limit} is applied to the PQ controller of the PV inverter. Another way to limit the power generated from the PV systems is by controlling the PV output current i_{pv}, as discussed in [23] and [24]. This approach is based on the characteristic of the PV arrays, where the PV output current i_{pv} is strongly dependent on the solar irradiance level, while the PV output voltage v_{pv} varies only in a small range during irradiance change. Thus, limiting the PV output current i_{pv} can effectively limit the PV output power P_{pv}. Alternatively, the CPG operation can also be realized by using the perturb and observe (P&O) algorithm, as proposed in [25]–[28]. In this method, the PV output voltage v_{pv} is continuously perturbed away from the MPP during the CPG operation mode in order to reduce the PV output power according to the set point (i.e., $P_{\text{pv}} = P_{\text{limit}}$).

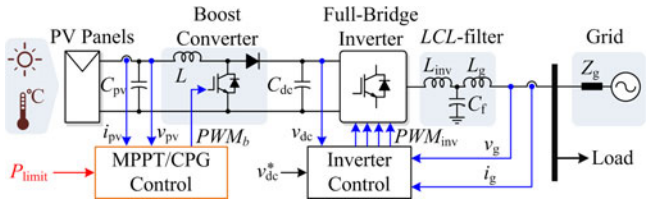

Fig. 3. Hardware schematics and overall control structure of a two-stage single-phase grid-connected PV system.

TABLE I
PARAMETERS OF THE TWO-STAGE SINGLE-PHASE PV SYSTEM (SEE FIG. 3)

PV rated power	3 kW
Boost converter inductor	$L = 1.8$ mH
PV-side capacitor	$C_{\text{pv}} = 1000\ \mu$F
DC-link capacitor	$C_{\text{dc}} = 1100\ \mu$F
LCL-filter	$L_{\text{inv}} = 4.8$ mH, $L_g = 2$ mH, $C_f = 4.3\ \mu$F
Switching frequency	Boost converter: $f_b = 16$ kHz, Full-bridge inverter: $f_{\text{inv}} = 8$ kHz
DC-link voltage	$v^*_{\text{dc}} = 450$ V
Grid nominal voltage (RMS)	$V_g = 230$ V
Grid nominal frequency	$\omega_0 = 2\pi \times 50$ rad/s

Nevertheless, the performance of the three CPG approaches has not yet been compared. Thus, it is difficult to justify which method is suitable to be implemented in industry and applied in the future grid codes. Besides, most of the literature studies only discuss the performance of the CPG strategy during the steady state (e.g., during a constant irradiance condition). In fact, depending on the mission profiles of the PV system (e.g., irradiance and temperature conditions), the operation mode transition between the MPPT and CPG can challenge the system performance, especially during a fluctuating irradiance condition (e.g., in a cloudy day). This will affect the system performance in terms of dynamics, accuracy, and stability of the CPG strategy, which have not yet been investigated so far.

In the light of the above issues, this paper first discusses about three different CPG strategies applied to two-stage single-phase PV systems. Then, the performance of the CPG strategies under both dynamic and steady-state conditions are benchmarked experimentally on a 3-kW two-stage single-phase grid-connected PV system, where real-field mission profiles are taken into consideration. Finally, conclusions are drawn from the comparison in Section V.

II. CONTROL STRUCTURE OF TWO-STAGE SINGLE-PHASE GRID-CONNECTED PV SYSTEMS

A. System Configuration

In most of the single-phase PV systems (e.g., rated power of 1–30 kW), a two-stage configuration is widely used [29], [30]. The system configuration and its control structure are shown in Fig. 3, where the system parameters are given in Table I. The PV arrays are connected to a boost converter, allowing a wide-range operation during both MPPT and CPG operations [31]. In other words, with the use of the two-stage configuration, the PV system can operate at a lower PV voltage v_{pv} (e.g., at the left side of the MPP in the case of the CPG operation),

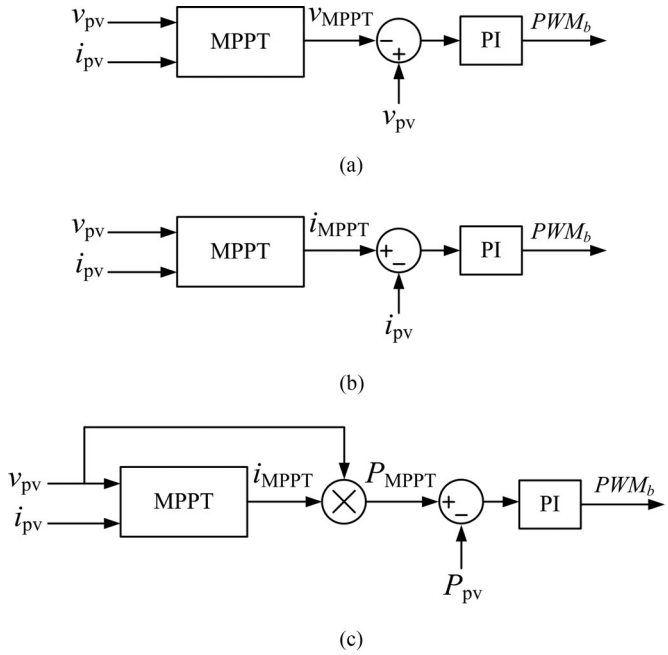

Fig. 4. Implementation of different MPPT controllers: (a) PV output voltage; (b) PV output current; and (c) PV output power, where PI represents a proportional-integral controller.

since the PV output voltage v_{pv} can be stepped up by the boost converter to match the required dc-link voltage (e.g., 450 V) for the PV inverter [29]. This may not be possible in the single-stage configuration, where the PV output voltage v_{pv} is directly fed to the PV inverter (i.e., $v_{pv} = v_{dc}$, with v_{dc} being the dc-link voltage). Practically, the dc-link voltage v_{dc} is required to be higher than the peak grid voltage level (e.g., 325 V) to ensure the power delivery [32].

In the boost converter stage, either the MPPT or CPG control can be implemented in order to control the power extraction from the PV arrays. Then, the extracted power is delivered to the ac grid through the control of the full-bridge inverter. In this case, the control of the full-bridge inverter keeps the dc-link voltage to be constant through the control of the injected grid current [33].

B. Boost Converter Controller

As aforementioned, the boost converter plays a major role to control the power extraction from the PV arrays. Therefore, it is important to discuss about the possible control structures for the boost converter, where the CPG strategies will be implemented. Usually, the MPPT algorithm (i.e., the P&O MPPT) is implemented in the boost converter. For example, the P&O MPPT algorithm can give either the reference PV voltage v_{MPPT} or current i_{MPPT} to control the boost converter. Thus, the MPPT is usually achieved by regulating either the PV output voltage v_{pv} or current i_{pv} according to the reference from the MPPT algorithm, as shown in Fig. 4(a) and (b). Alternatively, it is possible to achieve the MPPT through the control of the PV output power P_{pv}. In this case, the reference PV current from the MPPT algorithm i_{MPPT} is multiplied by the measured PV voltage v_{pv} in order to obtained the reference PV power P_{MPPT}, as shown in Fig. 4(c). In this way, the PV power P_{pv} is controlled directly at any time, making it possible and flexible to be modified according to the power set point (e.g., to realize the CPG operation). However, it should be mentioned that the variations in the PV voltage v_{pv} (e.g., due to the noise from measurements) can propagate to the reference P_{MPPT} through the direct multiplication and thereby decrease the tracking accuracy of the MPPT operation. Nevertheless, the tracking errors are with permissible limits, which will be experimentally verified in Section IV.

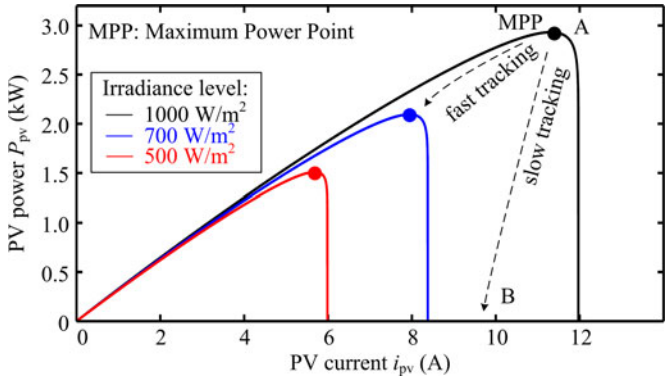

Fig. 5. Stability issues of the MPPT controller based on the PV output current due to the high slope (dP_{pv}/di_{pv}) at the right side of the MPP [34].

It is noteworthy to mention that tracking the MPP by controlling the PV current i_{pv} [i.e., Fig. 4(b)] is of less robustness [34]. This is due to the very steep slope (i.e., large dP_{pv}/di_{pv}) on the right side of the MPP in the power–current (P–I) curve of the PV arrays, as shown in Fig. 5. The operating point of the PV system may go into the short-circuit condition under a sudden decrease of the irradiance condition (if the MPPT algorithm cannot track fast enough, e.g., the PV system still operating at the same PV output current i_{pv}), when the PV output current is controlled [34]. This can be illustrated by the A→B trajectory in Fig. 5 when the irradiance level suddenly drops from 1000 to 700 W/m^2. This stability issue will be observed in a CPG control scheme, which is based on the control structure in Fig. 4(b).

III. CPG Strategies

Basically, the CPG strategy needs to regulate the operating point of the PV system at the CPPs in order to achieve a constant power production. According to the P–V characteristic curve of the PV arrays shown in Fig. 2, there are two possible operating points—CPP-L and CPP-R—for the CPG mode at a certain power level (i.e., P_{limit}) and a certain irradiance level. However, the CPPs continuously change (i.e., different PV voltage and PV current) under a changing irradiance condition, according to the P–V curve of the PV arrays. Thus, the CPG strategy has to be able to follow the change in the P–V curve and track the CPP in the case of the CPG operation. Generally, the demands for the CPG control schemes are as follows.

1) In the steady-state CPG operation, the CPG strategies should keep the PV systems operating at one of the CPPs with minimum deviations, in order to minimize the power losses in the steady state.

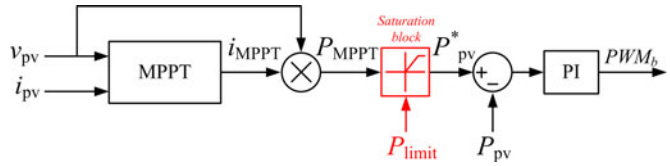

Fig. 6. Control structure of the CPG scheme based on a power control (P-CPG).

2) Under a changing irradiance condition (e.g., in a cloudy day), the CPG control scheme should be able to track either the MPP or the CPP, depending on the operating mode, and at the same time ensure a stable transition.

Accordingly, three previously mentioned CPG strategies are adapted to two-stage single-phase PV systems and are discussed in the following based on a power control method (P-CPG), a current limit method (I-CPG), and the P&O algorithm (P&O-CPG), where the above demands are taken as the benchmarking criteria.

A. CPG Based on a Power Control Method (P-CPG)

Limiting the PV output power through the closed-loop power control is one of the most commonly used solutions to achieve the CPG control in the previous work [15], [19]. In order to realize this control method in the two-stage single-phase PV system, the boost converter needs to directly control the PV output power during operation. As mentioned previously, it is possible to directly control the PV output power P_{pv} during the MPPT operating mode by employing the control scheme in Fig. 4(c), where the reference PV power in the MPPT mode P_{MPPT} is obtained by multiplying the reference current i_{MPPT} from the MPPT algorithm with the PV voltage v_{pv}. Regarding the CPG operation, a saturation block is added to the control scheme in Fig. 4(c) in order to limit the reference PV power P^*_{pv} to a certain power level P_{limit}, as shown in Fig. 6. Namely, when the reference PV power from the MPPT algorithm P_{MPPT} reaches the level of power limit P_{limit}, the saturation block will keep the power reference to be constant, i.e., $P^*_{pv} = P_{limit}$, and the PV system enters into the CPG mode. Otherwise, if the reference PV power from the MPPT algorithm P_{MPPT} is less than the power limit P_{limit}, the saturation block will not be activated, and the PV system will operate in the MPPT mode with a maximum power injection (i.e., $P^*_{pv} = P_{MPPT}$), which is equivalent to the MPPT controller in Fig. 4(c). The operational principle can be further summarized as

$$P^*_{pv} = \begin{cases} P_{MPPT}, & \text{when} \quad P_{MPPT} \le P_{limit} \\ P_{limit}, & \text{when} \quad P_{MPPT} > P_{limit} \end{cases} \tag{2}$$

where P_{MPPT} is the maximum available power (according to the MPPT operation), and P_{limit} is the power limit, as defined previously.

B. CPG Based on a Current Limit Method (I-CPG)

Another way to control the PV output power is through the control of the PV output current i_{pv}, as discussed in [23] and [24]. This is due to the fact that the PV voltage v_{pv} only varies in a small range during the irradiance change in the operating region on the right side of the MPP (at the CPP-R), as shown in Fig. 7. Therefore, the PV output power P_{pv} can effectively be controlled through the PV output current i_{pv} in this region. From the control scheme in Fig. 4(b), it is possible to achieve a CPG operation by limiting the reference current from the MPPT algorithm i_{MPPT} according to $i_{limit} = P_{limit}/v_{pv}$ when calculating the reference PV output current i^*_{pv}. The control structure of the I-CPG method is shown in Fig. 8, and the power limit P_{limit} corresponds to the rectangular area under the CPP-R in Fig. 7.

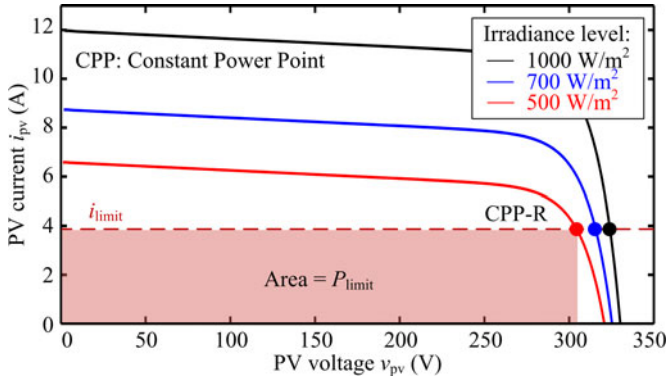

Fig. 7. Operational principle of the CPG scheme based on a current limit (I-CPG).

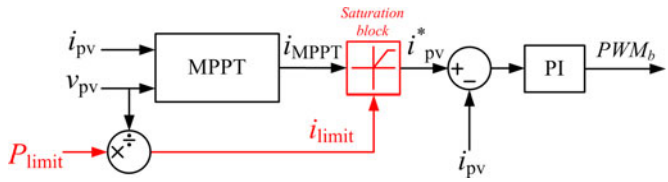

Fig. 8. Control structure of the CPG scheme based on a current limit (I-CPG).

According to the CPG concept in (1), the performance of the controller during the MPPT operation should not be diminished by the current limit. This can be ensured when considering

$$\frac{P_{MPPT}}{v_{pv}} \le \frac{P_{limit}}{v_{pv}}$$

and thus

$$i_{MPPT} \le i_{limit}$$

where it can be seen that the current limit will not be activated as long as $P_{MPPT} \le P_{limit}$, and the I-CPG method in the MPPT mode is simply equivalent to the MPPT controller in Fig. 4(b).

C. CPG Based on the P&O Algorithm (P&O-CPG)

A CPG operation can also be realized by means of a P&O algorithm [25]–[28]. This method is based on the MPPT control structure in Fig. 4(a), where the PV voltage v_{pv} is controlled. In this approach, the modification is done at the control algorithm when determining the reference PV voltage v^*_{pv}. More precisely, during the MPPT operation, the reference PV voltage v^*_{pv} is set from the MPPT algorithm (i.e., P&O MPPT). However, in the

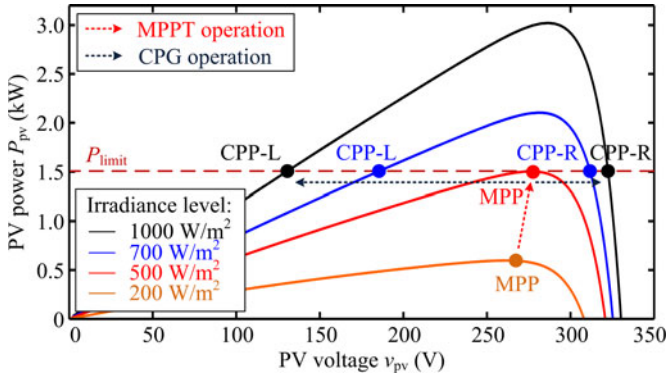

Fig. 9. Operational principle of the CPG scheme based on the P&O algorithm (P&O-CPG).

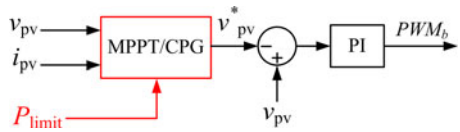

Fig. 10. Control structure of the CPG scheme based on the P&O algorithm (P&O-CPG).

case of the CPG operation, the PV voltage v_{pv} is continuously perturbed toward one CPP, i.e., $P_{pv} = P_{limit}$, as illustrated in Fig. 9. After a number of iterations, the operating point will be reached and oscillate around the corresponding CPP. Notably, the two-stage PV system with the P&O-CPG control can operate at either the CPP-L or the CPP-R, depending on the perturbation direction of the algorithm. However, the power oscillation in the steady state is larger at the CPP-R compared to that at the CPP-L due to the high slope of the P–V curve on the right side of the MPP (i.e., large dP_{pv}/dv_{pv}). This large power oscillation will decrease the tracking accuracy and increase the energy losses as well as the power fluctuations in the steady state, which should be avoided. On the other hand, the operating region at the CPP-L requires a higher conversion ratio (i.e., v_{dc}/v_{pv}) which may affect the boost converter efficiency [35]. The control structure of the algorithm is shown in Fig. 10, where the reference PV voltage v^*_{pv} can be expressed as

$$v^*_{pv} = \begin{cases} v_{MPPT}, & \text{when} \quad P_{pv} \le P_{limit} \\ v_{pv} - v_{step}, & \text{when} \quad P_{pv} > P_{limit} \end{cases} \tag{3}$$

if the PV system operates at the CPP-L, or

$$v^*_{pv} = \begin{cases} v_{MPPT}, & \text{when} \quad P_{pv} \le P_{limit} \\ v_{pv} + v_{step}, & \text{when} \quad P_{pv} > P_{limit} \end{cases} \tag{4}$$

if the PV system operates at the CPP-R, where v_{MPPT} is the reference voltage from the MPPT algorithm (i.e., the P&O MPPT algorithm) and v_{step} is the perturbation step size.

IV. Benchmarking of CPG Strategies

In order to benchmark the discussed CPG control strategies, experiments have been carried out referring to Fig. 3, where the experimental test rig is shown in Fig. 11. The performance of the

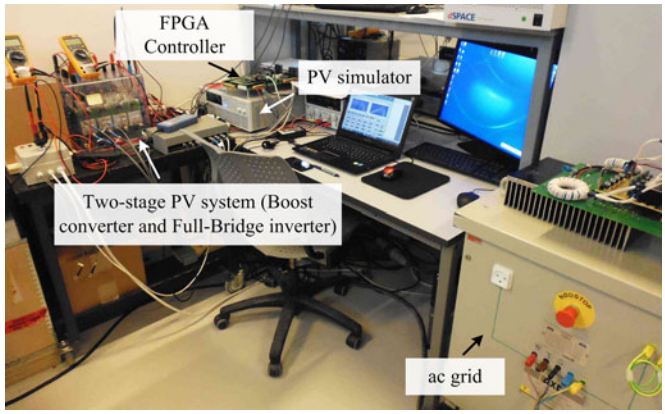

Fig. 11. Experimental setup of the two-stage grid-connected PV system.

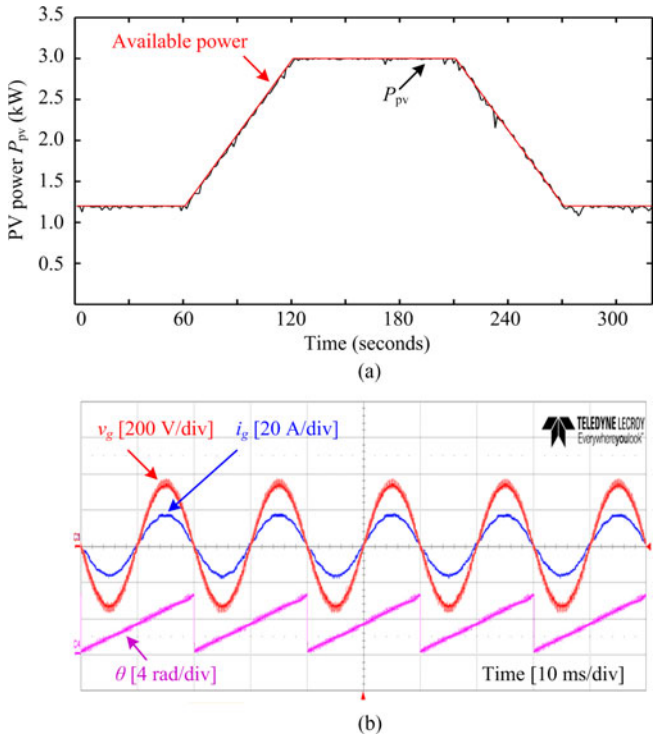

Fig. 12. Performance of the two-stage single-phase grid-connected PV system. (a) PV power extraction during the MPPT operation. (b) Grid voltage v_g, grid current i_g, and the phase angle θ during the steady-state MPPT operation (3 kW).

two-stage single-phase PV system during the MPPT operation is demonstrated in Fig. 12(a). Here, the sampling frequency of the MPPT (and also CPG) algorithms is chosen as 10 Hz (which is a typical sampling rate of the MPPT algorithm [36]). For the PV inverter controller, the dc-link voltage v_{dc} is regulated at 450 ± 5 V and the extracted power is delivered to a single-phase 50-Hz ac grid with a peak voltage of 325 V, as can be seen from Fig. 12(b).

In the experiments, a 3-kW PV simulator has been adopted, where irradiance and ambient temperature profiles can be programed to emulate the behavior of real PV arrays in different operating conditions. First, the performance of the CPG strategies is examined with a slow changing trapezoidal solar irradiance

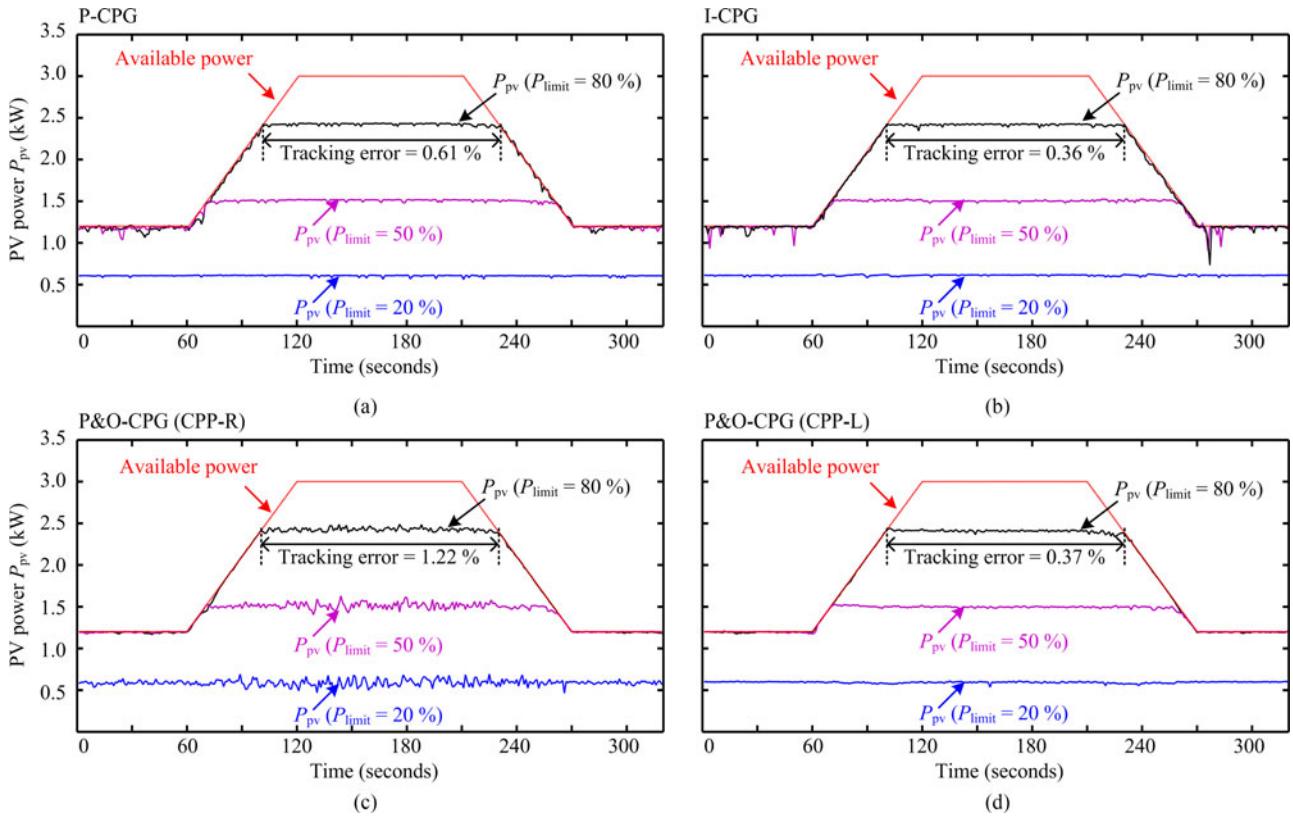

Fig. 13. Experimental results of the CPG scheme based on (a) the power control, (b) the current limit, (c) the P&O at the CPP-R, and (d) the P&O at the CPP-L under a slow changing irradiance condition. The tracking error is calculated from the difference between the actual PV output power $P_{\rm pv}$ and its set point $P_{\rm limit} = 80\%$ during the CPG mode (i.e., $|P_{\rm pv} - P_{\rm limit}|$) and then divided by the total energy yield.

profile in Fig. 13, where three different values of power limit $P_{\rm limit}$ (i.e., 20%, 50%, and 80% of the rated power) are used to verify the feasibility of the CPG strategies under various set points. Then, a fast changing trapezoidal solar irradiance profile in Fig. 14 is adopted in order to challenge the dynamic of the CPG strategy and to observe the behavior of the algorithm during the operating mode transition (e.g., from MPPT to CPG mode). Furthermore, two real-field solar irradiance and ambient temperature profiles are also programed in order to examine the performance of the CPG algorithms in the real operation, where $P_{\rm limit} = 1.5$ kW (i.e., 50% of the rated power). A clear day irradiance condition is used in Fig. 15, where the solar irradiance level changes relatively slowly and smoothly. In this condition, the CPG strategy mostly operates under the steady-state condition. In contrast, the dynamic performance of the CPG strategy can clearly be seen during the fluctuating irradiance condition in Fig. 16, where the cloudy day irradiance profile is emulated. During the above tests, the average tracking error (in percentage of the total energy yield) during the CPG mode is also provided in the same figure. The tracking error is calculated from the difference between the actual PV output power and its set point (i.e., $|P_{\rm pv} - P_{\rm limit}|$) and then divided by the total energy yield in order to make it comparable for different test conditions. This parameter can be used for comparing the tracking accuracy of different CPG strategies numerically. For instance, a large value of tracking error indicates a violation of the CPG constraint (i.e., $P_{\rm pv} > P_{\rm limit}$) and/or significant energy losses (i.e., $P_{\rm pv} < P_{\rm limit}$). Fig. 17 shows an example of the operating trajectories of the CPG strategies, where the irradiance condition in Fig. 13 is used. The detailed discussion about the results is given and benchmarked in the following.

A. Dynamic Responses

The dynamic responses can be observed during the CPG to MPPT transition and vice versa. For the trapezoidal irradiance condition, this transition occurs when the available power reaches the level of power limit $P_{\rm limit}$. In Fig. 13, all the CPG strategies have a smooth transition, since the irradiance changes relatively slowly. However, in the case of fast changing solar irradiance in Fig. 14, the dynamics of the CPG strategies are more challenged to follow the changes in the CPP. It can be observed from Fig. 14(c) and (d) that the P&O-CPG scheme presents large power overshoots during the MPPT to CPG transition. This is due to the fact that the P&O-CPG scheme is an iteration-based method, which requires a number of iterations in order to reach the corresponding CPP. A long-term dynamic response can be examined with the cloudy day irradiance condition in Fig. 16, where PV output power is continuously fluctuating. In this condition, similar power overshoots also appear in the P&O-CPG algorithm as it can be seen in Fig. 16(c) and (d). In contrast, the P- and I-CPG algorithms can regulate the PV output power to be constant almost without any overshoots during both short-term (i.e., Fig. 14) and long-term (i.e., Fig. 16) fast changing

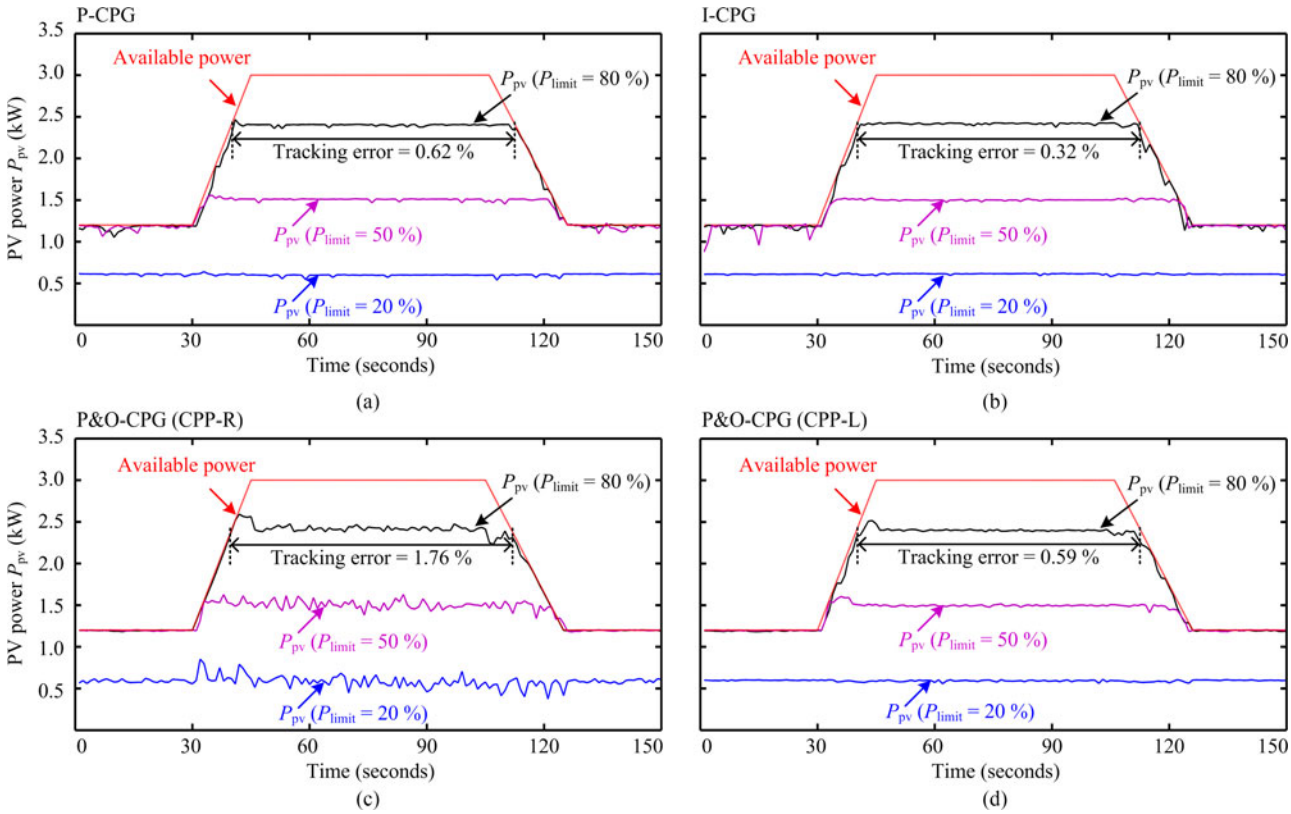

Fig. 14. Experimental results of the CPG scheme based on (a) the power control, (b) the current limit, (c) the P&O at the CPP-R, and (d) the P&O at the CPP-L under a fast changing irradiance condition. The tracking error is calculated from the difference between the actual PV output power P_{pv} and its set point $P_{\text{limit}} = 80\%$ during the CPG mode (i.e., $|P_{\text{pv}} - P_{\text{limit}}|$) and then divided by the total energy yield.

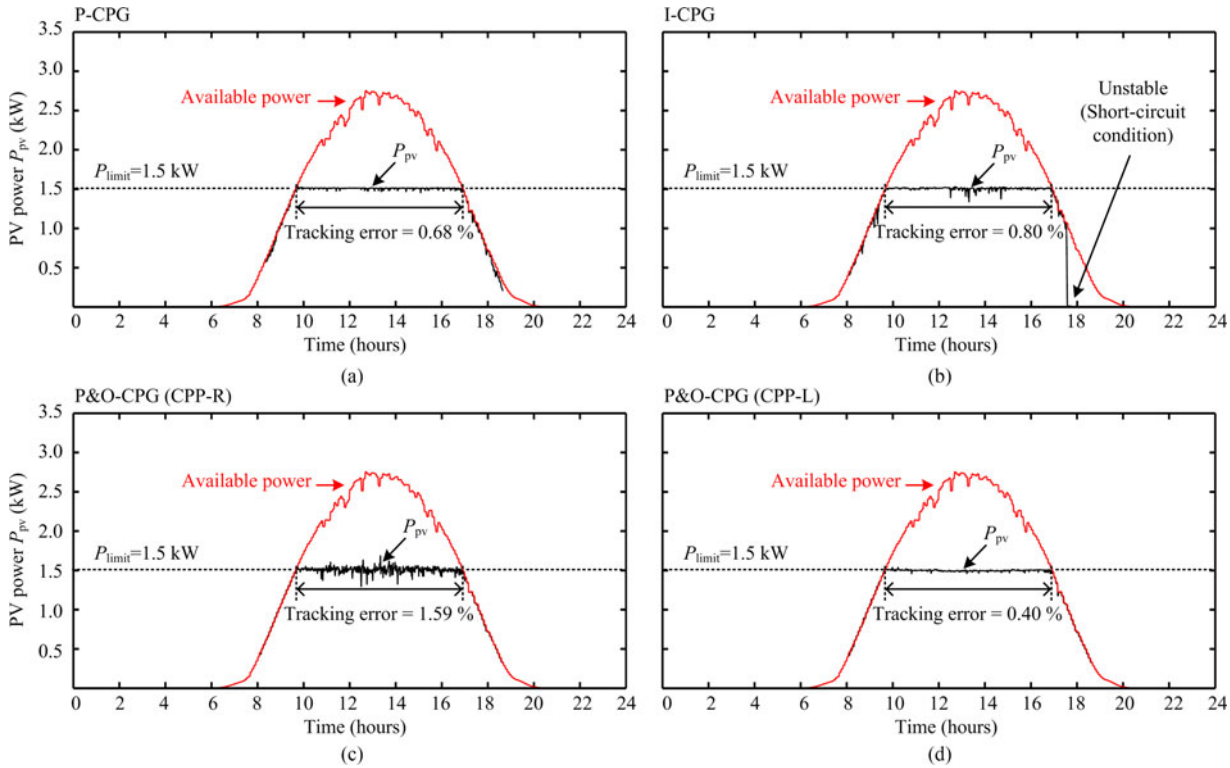

Fig. 15. Experimental results of the CPG scheme based on (a) the power control, (b) the current limit, (c) the P&O at the CPP-R, and (d) the P&O at the CPP-L under a clear day condition. The tracking error is calculated from the difference between the actual PV output power P_{pv} and its set point $P_{\text{limit}} = 1.5$ kW during the CPG mode (i.e., $|P_{\text{pv}} - P_{\text{limit}}|$) and then divided by the total energy yield.

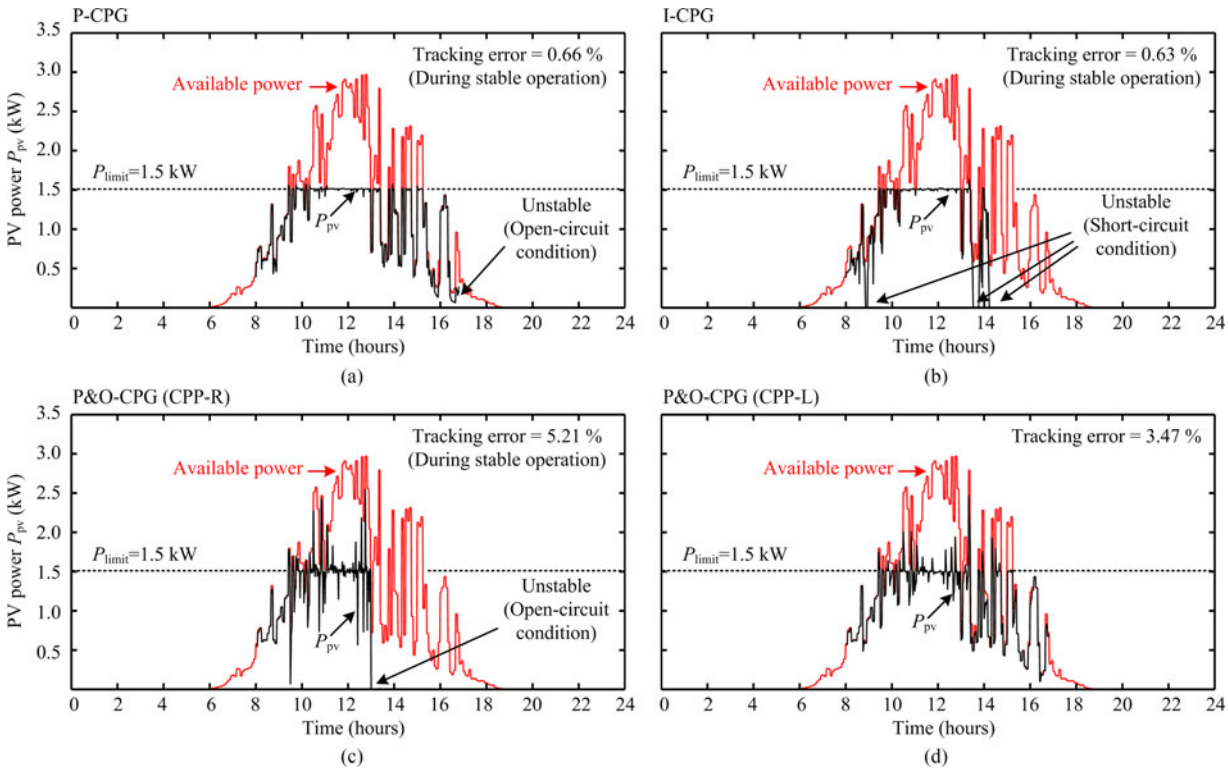

Fig. 16. Experimental results of the CPG scheme based on (a) the power control, (b) the current limit, (c) the P&O at the CPP-R, and (d) the P&O at the CPP-L under a cloudy day condition. The tracking error is calculated from the difference between the actual PV output power P_{pv} and its set point $P_{limit} = 1.5$ kW during the stable CPG mode (i.e., $|P_{pv} - P_{limit}|$) and then divided by the total energy yield.

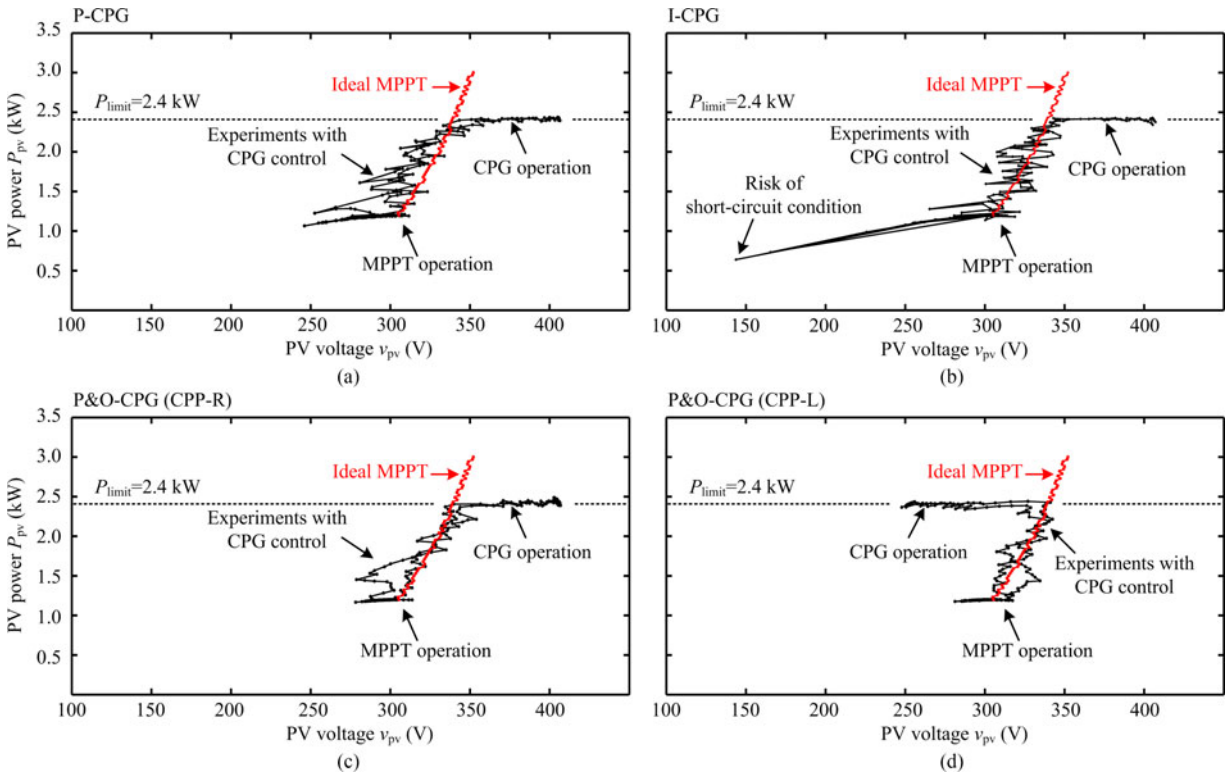

Fig. 17. Trajectory of the operating point of the CPG scheme based on (a) the power control, (b) the current limit, (c) the P&O at the right side of the MPP, and (d) the P&O at the left side of the MPP under a slow changing irradiance condition (see Fig. 13), when $P_{limit} = 2.4$ kW.

irradiance conditions. This fast dynamic performance is achieved because the P- and I-CPG strategies directly regulate the corresponding reference PV power $P_{\rm pv}$ (i.e., P-CPG) or PV current $i_{\rm pv}$ (i.e., I-CPG) through the close-loop control during the CPG mode. In other words, the algorithms do not require iterations in order to reach the CPP.

B. Steady-State Responses

In the steady state, the CPG algorithm should regulate the PV power $P_{\rm pv}$ to be constant with minimum deviations, as discussed in Section III. This can be observed from Figs. 13 and 14 during the time period when the irradiance level is constant. A long-term steady-state performance can also be seen in Fig. 15, since the irradiance level changes slowly and smoothly in the clear day condition. The experimental results in the above conditions show that most of the CPG algorithms have a satisfactory steady-state performance, where the PV output power $P_{\rm pv}$ is limited according to the set point $P_{\rm limit}$ with very small deviations. However, when the P&O-CPG algorithm is employed to regulate the PV power at the right side of the MPP (i.e., at the CPP-R), large power oscillations appear, as shown in Figs. 13(c), 14(c), and 15(c). This is due to the large $dP_{\rm pv}/dv_{\rm pv}$ at the CPP-R (see Fig. 2). Actually, it can be noticed from Figs. 13(c) and 14(c) that the power oscillation becomes even larger at the low power limit level (e.g., when $P_{\rm limit} = 20\%$), as the slope $dP_{\rm pv}/dv_{\rm pv}$ increases when the operating point is further at the right side of the MPP.

C. Tracking Error

The tracking error is another important performance aspect of the CPG strategy, which indicates numerically how well the algorithm follows the change in the CPP during the CPG operation. In fact, the tracking error is a consequence of both the dynamic and steady-state responses, depending on the irradiance profile. For example, the tracking error in the steady state is dominant in the trapezoidal irradiance profiles in Figs. 13 and 14, since the time period of a constant irradiance is much longer than the ramp changing (considered only during the CPG mode). Therefore, the tracking errors of the P&O-CPG strategies when operating at the CPP-R in Fig. 13 are significantly higher than the other methods. It can also be noticed that the P&O-CPG strategies (both at the CPP-R and CPP-L) have larger errors in Fig. 14 compared to those in Fig. 13, while the tracking errors of the P- and I-CPG strategies remain almost at the same level. This increased tracking error is corresponding to the power overshoot in Fig. 14, as has been discussed previously. A similar trend is also observed in Figs. 15 and 16, where it can be seen that the tracking error of the P&O-CPG method during the cloudy day condition is significantly larger than the case during the clear day condition, while the P- and I-CPG strategies have almost the same tracking error. Notably, only the tracking error during stable CPG operation is considered in this case.

D. Stability

Stability is one of the most important aspects for the CPG control schemes, since the PV system should be able to continuously deliver power to the grid regardless of the operating condition. Thus, the presented CPG strategies are also benchmarked in terms of stability. For the PV systems, instability may occur during a fast decreasing irradiance condition, which can be further divided into two cases: the short-circuit condition and the open-circuit condition. The occurrence of the short-circuit instability and its mechanism have been previously discussed in Section II. This type of instability can occur with the I-CPG strategy where the PV current $i_{\rm pv}$ is regulated, as can be observed in Figs. 15(b) and 16(b). In fact, it can also be seen from the operating trajectories in Fig. 17(b) that the operating point of the PV system almost goes into the short-circuit condition during a decreasing irradiance level. Another case of instability is when the operating point falls into (and stay at) the open-circuit condition. This open-circuit instability can occur in the case of the P- and P&O-CPG algorithms when the operating point is chosen at the CPP-R. The operating point may go into the open-circuit condition during a decreasing irradiance condition if the PV power is regulated too far at the right side of the MPP (i.e., at C), since the open-circuit voltage in the P–V curve decreases as the irradiance level drops (e.g., from 1000 to 200 W/m^2). The mechanism of the open-circuit instability is illustrated in Fig. 18 (i.e., C→D). Fig. 16(a) and (c) verifies that the P-CPG or the P&O-CPG at the right side of the MPP can go into instability during transients. In contrast, it can be seen in Figs. 15 and 16 that the P&O-CPG algorithm can always ensure a stable operation regardless of the irradiance conditions, only when the PV system operating point is regulated at the CPP-L. In this operating region, the sudden drops in the irradiance will not lead to either the short-circuit or open-circuit instability, as can be seen from Fig. 18 (i.e., A→B).

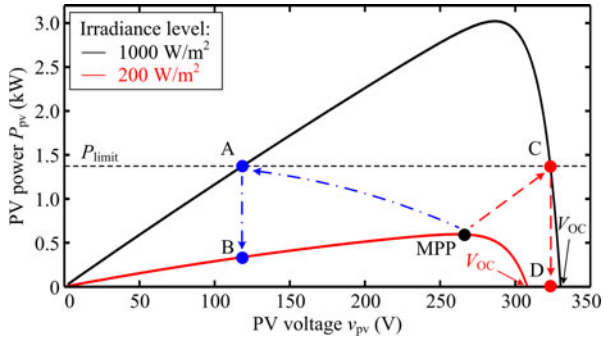

Fig. 18. Possible operating regions of the CPG strategy, where the instability issue during the fast decreasing irradiance condition is illustrated.

E. Complexity

When comparing all the above CPG strategies, it is found that the I-CPG algorithm has the simplest control structure, where only one additional current limiter needs to be added to the original MPPT controller in Fig. 4(b). Besides, the calculation of the $i_{\rm limit}$ is also simple by dividing $P_{\rm limit}$ by the measured PV voltage $v_{\rm pv}$. The control structure of the P-CPG algorithm is more complicated, basically due to the MPPT controller in Fig. 4(c). In the case of the P&O-CPG algorithm, the modification needs to be done at the MPPT algorithm level, as can be seen from

TABLE II
BENCHMARKING OF THE CPG ALGORITHMS

CPG Strategy	Dynamic Responses	Steady-state Responses	Tracking Error	Stability	Complexity
Power control (P-CPG)	+ +	+	+	−	−
Current limit (I-CPG)	+ +	+	+	− −	+ +
P&O-CPG at CPP-R	− −	− −	− −	−	−
P&O-CPG at CPP-L	− −	+ +	−	+ +	−

Note: the more +, the less tracking error, better stability, and less complexity.

Fig. 10. This makes the design of a P&O-CPG controller more complicated than the other two CPG algorithms.

Table II further summarizes a comparison of the results of the CPG control schemes in terms of dynamic and steady-state performances, tracking error, stability, and complexity. The benchmarking results have validated the effectiveness of the CPG strategies under various test conditions. It turns out that the P-CPG strategy can achieve very fast dynamics, especially during fast changing irradiance condition, compared to the other strategies. However, this method may induce instability during the sudden irradiance drops, if the PV system operates at a low level of power limit (i.e., CPP-R is far away from MPP). Thus, it is suitable to be implemented in the PV system with historical fast changing irradiance profiles (e.g., small scale PV system with cloudy conditions), and a high level of power limit (i.e., operate at the CPP-R close to the MPP), in order to minimize the risk of instability. On the other hand, the P&O-CPG algorithm (when operating at the CPP-L) is the most suitable approach to realize the CPG control practically due to its robustness and feasible to be used for the future grid codes. This method is also suitable when a wide range of CPG operation (e.g., at different level of power limit) is required. However, the tracking error of the P&O-CPG algorithm increases during fast changing irradiance conditions, which is a tradeoff that should be considered.

V. CONCLUSION

In this paper, three CPG control solutions for single-phase grid-connected PV systems have been presented. A benchmarking of the three CPG control methods has also been conducted in terms of dynamic and steady-state performances, tracking error, stability, and complexity. Comparisons have revealed that the CPG strategy based on a current limit method (I-CPG) has the simplest control structure. Additionally, the power control based CPG scheme (P-CPG) has fast dynamics and good steady-state responses. However, instability may occur in both I-CPG and P-CPG methods during the operational mode transition, e.g., in the case of a fast change in the solar irradiance. It can be concluded that the CPG based on the P&O algorithm (P&O-CPG) is the best one in terms of high robustness among the three CPG strategies once the PV system is operating at the left side of the MPP.

REFERENCES

[1] REN21, "Renewables 2015: Global Status Report (GRS)," 2015. [Online]. Available: http://www.ren21.net/
[2] Fraunhofer ISE, "Recent Facts about Photovoltaics in Germany," May 19, 2015. [Online]. Available: http://www.pv-fakten.de/
[3] Solar Power Europe, "Global Market Outlook For Solar Power 2015–2019," 2015. [Online]. Available: http://www.solarpowereurope.org/
[4] Y. Yang, P. Enjeti, F. Blaabjerg, and H. Wang, "Wide-scale adoption of photovoltaic energy: Grid code modifications are explored in the distribution grid," *IEEE Ind. Appl. Mag.*, vol. 21, no. 5, pp. 21–31, Sep. 2015.
[5] S. Eftekharnejad, V. Vittal, G. Heydt, B. Keel, and J. Loehr, "Impact of increased penetration of photovoltaic generation on power systems," *IEEE Trans. Power Syst.*, vol. 28, no. 2, pp. 893–901, May 2013.
[6] R. Tonkoski, D. Turcotte, and T. El-Fouly, "Impact of high PV penetration on voltage profiles in residential neighborhoods," *IEEE Trans. Sustain. Energy*, vol. 3, no. 3, pp. 518–527, Jul. 2012.
[7] T. Stetz, J. von Appen, F. Niedermeyer, G. Scheibner, R. Sikora, and M. Braun, "Twilight of the grids: The impact of distributed solar on Germany's energy transition," *IEEE Power Energy Mag.*, vol. 13, no. 2, pp. 50–61, Mar. 2015.
[8] D. Maxwell, "Parts of Northern Ireland's electricity grid overloaded," *BBC News NI*, 2013. [Online]. Available: http://www.bbc.com/.
[9] E. Reiter, K. Ardani, R. Margolis, and R. Edge, "Industry perspectives on advanced inverters for us solar photovoltaic systems: Grid benefits, deployment challenges, and emerging solutions," Nat. Renew. Energy Lab., Golden, CO, USA, Tech. Rep. no. NREL/TP-7A40-65063, 2015.
[10] T. Stetz, F. Marten, and M. Braun, "Improved low voltage grid-integration of photovoltaic systems in Germany," *IEEE Trans. Sustain. Energy*, vol. 4, no. 2, pp. 534–542, Apr. 2013.
[11] A. Ahmed, L. Ran, S. Moon, and J.-H. Park, "A fast PV power tracking control algorithm with reduced power mode," *IEEE Trans. Energy Convers.*, vol. 28, no. 3, pp. 565–575, Sep. 2013.
[12] T. Caldognetto, S. Buso, P. Tenti, and D. Brandao, "Power-based control of low-voltage microgrids," *IEEE Trans. Emerg. Sel. Topics Power Electron.*, vol. 3, no. 4, pp. 1056–1066, Dec. 2015.
[13] German Federal Law: Renewable Energy Sources Act (Gesetz fur den Vorrang Erneuerbarer Energien), BGBl Std., Document No.: BGBl. I S. 1066, Jul. 2014.
[14] Energinet.dk, "Technical regulation 3.2.2 for PV power plants with a power output above 11 kW," Energinet.dk, Erritsø, Denmark, Tech. Rep. no. 14/17997-39, 2015.
[15] Y. Yang, H. Wang, F. Blaabjerg, and T. Kerekes, "A hybrid power control concept for PV inverters with reduced thermal loading," *IEEE Trans. Power Electron.*, vol. 29, no. 12, pp. 6271–6275, Dec. 2014.
[16] H. Beltran, E. Bilbao, E. Belenguer, I. Etxeberria-Otadui, and P. Rodriguez, "Evaluation of storage energy requirements for constant production in PV power plants," *IEEE Trans. Ind. Electron.*, vol. 60, no. 3, pp. 1225–1234, Mar. 2013.
[17] W. A. Omran, M. Kazerani, and M. M. A. Salama, "Investigation of methods for reduction of power fluctuations generated from large grid-connected photovoltaic systems," *IEEE Trans. Energy Convers.*, vol. 26, no. 1, pp. 318–327, Mar. 2011.
[18] A. Sangwongwanich, Y. Yang, F. Blaabjerg, and H. Wang, "Benchmarking of constant power generation strategies for single-phase grid-connected photovoltaic systems," in *Proc. IEEE Appl. Power Electron. Conf. Expo.*, Mar. 2016, pp. 370–377.
[19] C. Rosa, D. Vinikov, E. Romero-Cadaval, V. Pires, and J. Martins, "Low-power home PV systems with MPPT and PC control modes," in *Proc. Int. Conf. Workshop Compat. Power Electron.*, Jun. 2013, pp. 58–62.
[20] W. Cao *et al.*, "Two-stage PV inverter system emulator in converter based power grid emulation system," in *Proc. IEEE Energy Convers. Congr. Expo.*, Sep. 2013, pp. 4518–4525.
[21] F. Olivier, P. Aristidou, D. Ernst, and T. V. Cutsem, "Active management of low-voltage networks for mitigating overvoltages due to photovoltaic units," *IEEE Trans. Smart Grid*, vol. 7, no. 2, pp. 926–936, Mar. 2016.

[22] F. Yang, L. Yang, and X. Ma, "An advanced control strategy of PV system for low-voltage ride-through capability enhancement," *Sol. Energy*, vol. 109, pp. 24–35, 2014.
[23] A. Urtasun, P. Sanchis, and L. Marroyo, "Limiting the power generated by a photovoltaic system," in *Proc. 10th Int. Multi-Conf. Syst., Signals Devices*, Mar. 2013, pp. 1–6.
[24] Y. Chen, C. Tang, and Y. Chen, "PV power system with multi-mode operation and low-voltage ride-through capability," *IEEE Trans. Ind. Electron.*, vol. 62, no. 12, pp. 7524–7533, Dec. 2015.
[25] R. G. Wandhare and V. Agarwal, "Precise active and reactive power control of the PV-DGS integrated with weak grid to increase PV penetration," in *Proc. IEEE 40th Photovolt. Spec. Conf.*, Jun. 2014, pp. 3150–3155.
[26] M. Mirhosseini, J. Pou, and V. Agelidis, "Single- and two-stage inverter-based grid-connected photovoltaic power plants with ride-through capability under grid faults," *IEEE Trans. Sustain. Energy*, vol. 6, no. 3, pp. 1150–1159, Jul. 2015.
[27] L. D. Watson and J. W. Kimball, "Frequency regulation of a microgrid using solar power," in *Proc. 26th Annu. IEEE Appl. Power Electron. Conf. Expo.*, Mar. 2011, pp. 321–326.
[28] A. Sangwongwanich, Y. Yang, and F. Blaabjerg, "High-performance constant power generation in grid-connected PV systems," *IEEE Trans. Power Electron.*, vol. 31, no. 3, pp. 1822–1825, Mar. 2016.
[29] S. B. Kjaer, J. K. Pedersen, and F. Blaabjerg, "A review of single-phase grid-connected inverters for photovoltaic modules," *IEEE Trans. Ind. Appl.*, vol. 41, no. 5, pp. 1292–1306, Sep. 2005.
[30] SMA, "Sunny Family 2010/2011," [Online]. Available: https://www.sma.de/en/products/solarinverters.html/
[31] H. Ghoddami and A. Yazdani, "A bipolar two-stage photovoltaic system based on three-level neutral-point clamped converter," in *Proc. IEEE Power Energy Soc. Gen. Meeting*, Jul. 2012, pp. 1–8.
[32] B. Yang, W. Li, Y. Zhao, and X. He, "Design and analysis of a grid-connected photovoltaic power system," *IEEE Trans. Power Electron.*, vol. 25, no. 4, pp. 992–1000, Apr. 2010.
[33] F. Blaabjerg, R. Teodorescu, M. Liserre, and A.V. Timbus, "Overview of control and grid synchronization for distributed power generation systems," *IEEE Trans. Ind. Electron.*, vol. 53, no. 5, pp. 1398–1409, Oct. 2006.
[34] N. Femia, G. Petrone, G. Spagnuolo, and M. Vitelli, *Power Electronics and Control Techniques for Maximum Energy Harvesting in Photovoltaic Systems*. Boca Raton, FL, USA: CRC Press, 2012.
[35] R. W. Erickson and D. Maksimovic, *Fundamentals of Power Electronics*, 2nd ed. Norwell, MA, USA: Kluwer, 2001.
[36] N. Femia, G. Petrone, G. Spagnuolo, and M. Vitelli, "Optimization of perturb and observe maximum power point tracking method," *IEEE Trans. Power Electron.*, vol. 20, no. 4, pp. 963–973, Jul. 2005.

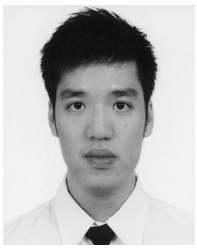

Ariya Sangwongwanich (S'15) received the B.Eng. degree in electrical engineering from Chulalongkorn University, Bangkok, Thailand, in 2013, and the M.Sc. degree in energy engineering from Aalborg University, Aalborg, Denmark, in 2015, where he is currently working toward the Ph.D. degree in electrical engineering.

His research interests include control of grid-connected converter, photovoltaic systems, reliability in power electronics, and high-power multilevel converters.

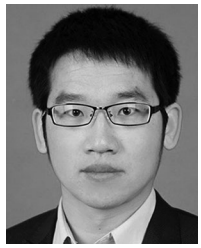

Yongheng Yang (S'12–M'15) received the postgraduate degree from Southeast University, Nanjing, China, in 2011; the B.Eng. degree from Northwestern Polytechnical University, Xi'an, China, in 2009; and the Ph.D. degree from Aalborg University, Aalborg, Denmark, in 2014, all in electrical engineering.

In 2013, he was a Visiting Scholar at Texas A&M University, College Station, TX, USA. Since 2014, he has been with the Department of Energy Technology, Aalborg University, where he is currently an Assistant Professor. His research interests include grid integration of renewable energy systems, power converter design, analysis and control, and reliability in power electronics.

Dr. Yang is a member of the IEEE Power Electronics Society Students and Young Professionals Committee. He served as a Guest Associate Editor of the IEEE JOURNAL OF EMERGING AND SELECTED TOPICS IN POWER ELECTRONICS and a Guest Editor of *Applied Sciences*. He is an Associate Editor of the *CPSS Transactions on Power Electronics and Applications*.

Frede Blaabjerg (S'86–M'88–SM'97–F'03) received the Ph.D. degree from Aalborg University, Aalborg, Denmark, in 1992.

He was at ABB-Scandia, Randers, Denmark, from 1987 to 1988, where he became an Assistant Professor in 1992, an Associate Professor in 1996, and a Full Professor of power electronics and drives in 1998. His current research interests include power electronics and its applications such as in wind turbines, photovoltaic systems, reliability, harmonics, and adjustable-speed drives.

Dr. Blaabjerg has received 17 IEEE Prize Paper Awards, the IEEE Power Electronics Society Distinguished Service Award in 2009, the European Power Electronic-Power Electronics and Motion Control (EPE-PEMC) Council Award in 2010, the IEEE William E. Newell Power Electronics Award in 2014, and the Villum Kann Rasmussen Research Award in 2014. He was the Editor-in-Chief of the IEEE TRANSACTIONS ON POWER ELECTRONICS from 2006 to 2012. He was nominated in 2014, 2015, and 2016 by Thomson Reuters to be among the most 250 cited researchers in engineering.

Huai Wang (S'07–M'12) received the B.E. degree in electrical engineering from the Huazhong University of Science and Technology, Wuhan, China, in 2007, and the Ph.D. degree in power electronics from the City University of Hong Kong, Hong Kong, in 2012.

He is currently an Associate Professor and a Research Thrust Leader with the Center of Reliable Power Electronics (CORPE), Aalborg University, Aalborg, Denmark. He was a Visiting Scientist at ETH Zurich, Zurich, Switzerland, from August to September 2014, and at the Massachusetts Institute of Technology (MIT), Cambridge, MA, USA, from September to November 2013. He was at the ABB Corporate Research Center, Switzerland, in 2009. His research addresses the fundamental challenges in modelling and validation of power electronic component failure mechanisms, and application issues in system-level predictability, condition monitoring, circuit architecture, and robustness design. He has contributed a few concept papers in the area of power electronics reliability, filed four patents on capacitive dc-link inventions, and co-edited a book.

Dr. Wang received the Richard M. Bass Outstanding Young Power Electronics Engineer Award from the IEEE Power Electronics Society in 2016, and the Green Talents Award from the German Federal Ministry of Education and Research in 2014. He is currently the Award Chair of the Technical Committee of the High Performance and Emerging Technologies, IEEE Power Electronics Society. He serves as an Associate Editor of *IET Power Electronics*, the IEEE JOURNAL OF EMERGING AND SELECTED TOPICS IN POWER ELECTRONICS, and the IEEE TRANSACTIONS ON POWER ELECTRONICS.